iScience

CellPress
OPEN ACCESS

Article

Limited TCR repertoire and *ENTPD1* dysregulation mark late-stage COVID-19

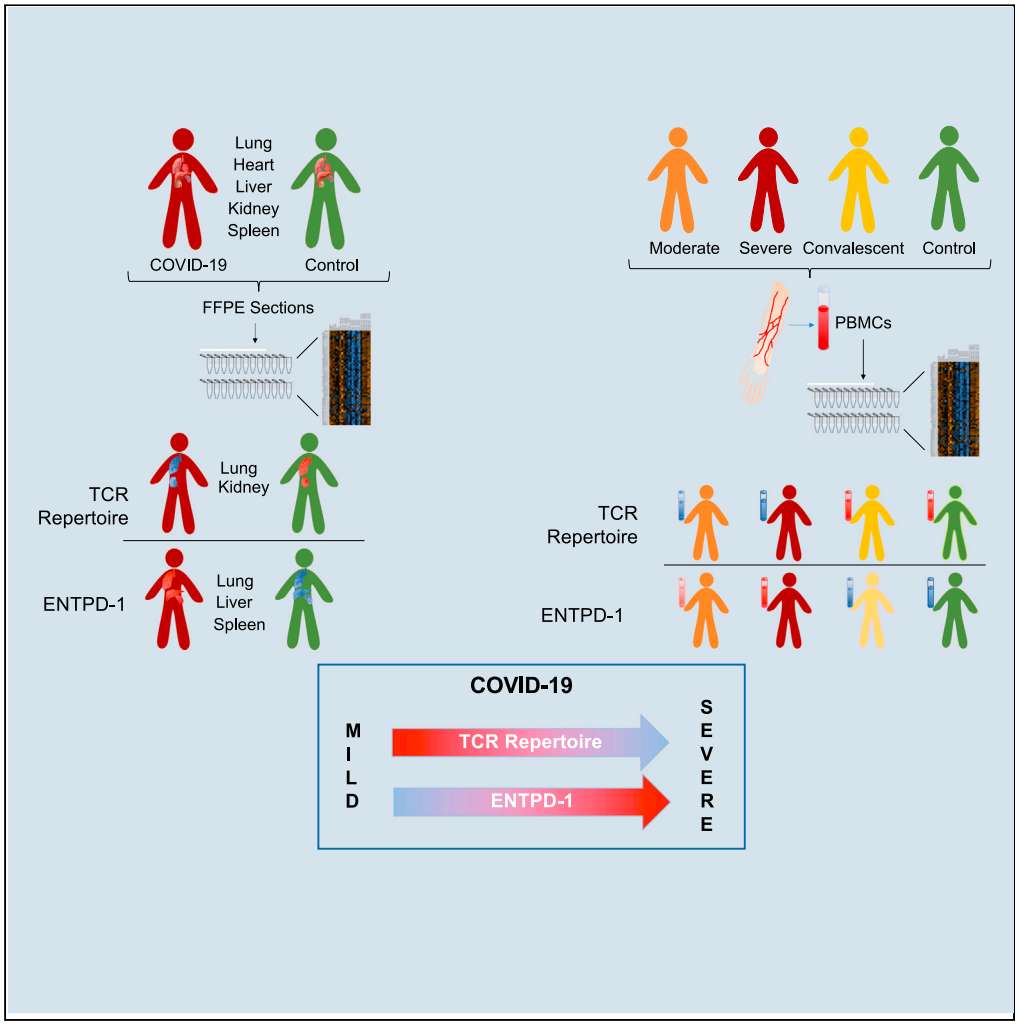

Na Wang, Marta Vuerich, Ahmadreza Kalbasi, ..., Shahzad Shaefi, Simon C. Robson, Maria Serena Longhi

mlonghi@bidmc.harvard.edu

Highlights

Transcriptome profiling of COVID-19 autoptic tissue and PBMC was carried out

There is limited TCR repertoire in lung, kidney and PBMC of severe COVID-19 cases

There are increased CD39 levels in PBMC of severe COVID-19 patients

High HIF-1a and STAT-3 and low CD39-antisense might be linked with CD39 increase

Wang et al., iScience 24, 103205
October 22, 2021
https://doi.org/10.1016/j.isci.2021.103205

iScience

CellPress
OPEN ACCESS

Article

Limited TCR repertoire and *ENTPD1* dysregulation mark late-stage COVID-19

Na Wang,[1,2,3,9] Marta Vuerich,[1,9] Ahmadreza Kalbasi,[1,9] Jonathon J. Graham,[1] Eva Csizmadia,[1] Zachary James Manickas-Hill,[4] Ann Woolley,[5] Clement David,[6] Eric M. Miller,[6] Kara Gorman,[6] Jonathan L. Hecht,[7] Shahzad Shaefi,[1] Simon C. Robson,[1,8] and Maria Serena Longhi[1,10,*]

SUMMARY

T cell exhaustion and dysfunction are hallmarks of severe COVID-19. To gain insights into the pathways underlying these alterations, we performed a comprehensive transcriptome analysis of peripheral-blood-mononuclear-cells (PBMCs), spleen, lung, kidney, liver, and heart obtained at autopsy from COVID-19 patients and matched controls, using the nCounter CAR-T-Characterization panel. We found substantial gene alterations in COVID-19-impacted organs, especially the lung where altered TCR repertoires are noted. Reduced TCR repertoires are also observed in PBMCs of severe COVID-19 patients. *ENTPD1/CD39*, an ectoenzyme defining exhausted T-cells, is upregulated in the lung, liver, spleen, and PBMCs of severe COVID-19 patients where expression positively correlates with markers of vasculopathy. Heightened *ENTPD1/CD39* is paralleled by elevations in *STAT-3* and *HIF-1α* transcription factors; and by markedly reduced *CD39*-antisense-RNA, a long-noncoding-RNA negatively regulating *ENTPD1/CD39* at the post-transcriptional level. Limited TCR repertoire and aberrant regulation of *ENTPD1/CD39* could have permissive roles in COVID-19 progression and indicate potential therapeutic targets to reverse disease.

INTRODUCTION

Coronavirus disease 2019 (COVID-19) is a potentially fatal multisystem inflammatory disease caused by the severe acute respiratory syndrome coronavirus-2 (SARS-CoV-2).

This serious illness has been associated with alterations in T cell immunity (Sette and Crotty, 2021), which vary according to the disease stage (Peng et al., 2020; Zhang et al., 2020). Aberrant features include CD8 T cell cytopenia (Laing et al., 2020), upregulation of HLA-DR and CD45RO activation markers and immune exhaustion (Kusnadi et al., 2021): a phenotype that becomes more pronounced with disease progression (Wang et al., 2020). Investigations at the transcriptional level have analyzed the single cell landscape of peripheral blood-derived lymphomononuclear cells in small patients' cohorts. These earlier studies have indicated HLA-class II downregulation (Wilk et al., 2020), increases in Fas-induced T cell apoptosis (Zhu et al., 2020) and decreased expression of genes associated with NK and CD8 T cell cytotoxicity in moderate to severe COVID-19 cases (Yao et al., 2021).

To gain better insights into the mechanistic pathways and gene signatures linked with these alterations, we have performed a comprehensive transcriptome analysis of peripheral blood mononuclear cells (PBMCs), spleen, lung, kidney, liver and heart obtained at autopsy from COVID-19 patients and matched controls. We report that restrictions in T cell receptor (TCR) repertoire and aberrant regulation of the *ENTPD1/CD39* ectoenzyme might underlie, at least in part, the T cell dysfunction and putative immune exhaustion observed in severe COVID-19.

RESULTS

Limited TCR repertoire in COVID-19

We used the nCounter CAR-T Characterization Panel (NanoString Technologies, Seattle, WA) (see Table S1) to profile 770 genes of 43 T cell-related pathway annotations in PBMCs and autoptic tissues, obtained from COVID-19 patients and controls. PBMCs were obtained from 45 COVID-19 patients, of whom 20 had

[1]Department of Anesthesia, Critical Care & Pain Medicine, Beth Israel Deaconess Medical Center, Harvard Medical School, 330 Brookline Avenue, Boston, MA 02215, USA

[2]Department of Hematology, Shandong Provincial Hospital Affiliated to Shandong First Medical University, 324 Jingwu Road, Jinan, Shandong 250021, China

[3]School of Medicine, Shandong University, 44 Wenhuaxilu, Jinan, Shandong 250021, China

[4]Ragon Institute of MGH, MIT and Harvard, 400 Technology Square, Cambridge, MA 02139, USA

[5]Division of Infectious Diseases, Brigham and Women's Hospital, 75 Francis Street, Boston, MA 02115, USA

[6]NanoString Technologies, 530 Fairview Avenue N, Seattle, WA 98109, USA

[7]Department of Pathology, Beth Israel Deaconess Medical Center, Harvard Medical School, 330 Brookline Avenue, Boston, MA 02215, USA

[8]Department of Medicine, Division of Gastroenterology, Beth Israel Deaconess Medical Center, Harvard Medical School, 330 Brookline Avenue, Boston, MA 02215, USA

[9]These authors contributed equally

[10]Lead contact

*Correspondence: mlonghi@bidmc.harvard.edu

https://doi.org/10.1016/j.isci.2021.103205

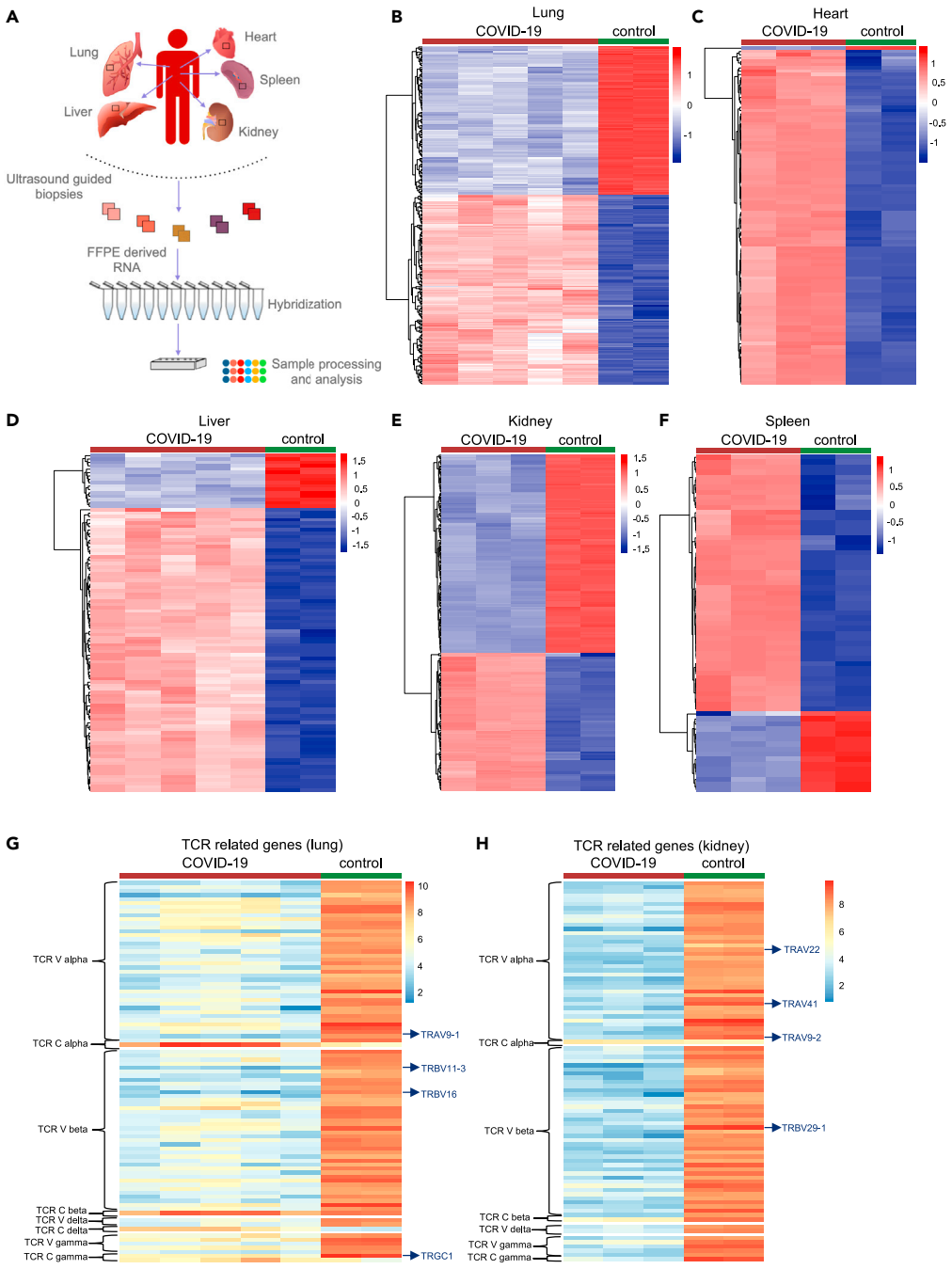

Figure 1. Limited TCR repertoire in lung, kidney, and PBMCs of severe COVID-19 patients

(A) Ultrasound-guided biopsies of autoptic lung (n = 5), heart (n = 3), liver (n = 5), kidney (n = 3), and spleen (n = 3) were obtained from COVID-19 patients and non-COVID-19 controls (n = 2 for all organs). Tissue samples were placed in formalin and, 24 h later, processed and paraffin embedded. Total RNA was extracted and subjected to hybridization prior to NanoString processing and profiling.

(B–F) Heatmaps showing differentially expressed genes (DEGs) included in the nCounter CAR-T Characterization Panel in lung (B), heart (C), liver (D), kidney (E), and spleen (F) from COVID-19 patients versus controls. Upregulated and downregulated genes are shown in red and blue, respectively. DEGs were defined based on p value $\leq 10^{-4}$ (false discovery rate <0.05 in all cases).

Figure 1. *Continued*
(G and H) Heatmaps representing TCR variable and constant alpha, beta, gamma and delta gene sets in lung (G) and kidney (H) of COVID-19 patients versus controls are shown. Upregulated and downregulated genes are represented in red and blue, respectively. Those genes undergoing the most substantial changes in COVID-19 lung and kidney are indicated. Data represented in (G) and (H) refer to gene expression normalized to the housekeeping genes included in the nCounter CAR-T genes. All samples subjected to NanoString analysis were run in triplicate and experiments performed independently three times. See also Figures S1 and S2.

moderate disease, 15 had severe disease and 10 were convalescents, and from 10 healthy controls. Autopsy tissues included biopsies from lung, heart, liver, kidney, and spleen of 5 COVID-19 patients and 2 controls, for a total of 29 samples. Demographic and clinical data of COVID-19 patients are summarized in Table S2.

When analyzing autopsy tissue (Figure 1A), the gene repertoires in COVID-19 lung, heart, liver, kidney, and spleen differed substantially from those of control tissues, as indicated in the heatmaps presented in Figures 1B–1F. Analysis of signature scores indicated that, compared with controls, organs from COVID-19 patients underwent most substantial changes (i.e. $\geq$ 50% genes, for which the p value was $\leq 10^{-4}$ when compared with healthy control samples) in the expression of genes included in metabolic pathways, namely oxidative phosphorylation (lung, heart, liver, and kidney), glycolysis (lung) and glutamine metabolism (kidney) (see Figures S1A–S1D and S2A–S2F). In addition to these metabolic alterations, likely resulting in the production of aberrantly high levels of ATP, we noted that COVID-19 lungs displayed upregulation of genes associated with Th9 cell immunity (see Figures S1A and S2G), which was found upregulated in peripheral blood samples of COVID-19 convalescents, even 2 months after recovery (Ortologas-Stavrou et al., 2020); whereas in COVID-19 spleen genes related to memory cell markers were among those mostly upregulated (see Figure S1E).

Notably, genes associated with TCR repertoire (see Table S3) were among the most downregulated in COVID-19 lung and kidney (Figures 1G, 1H, S1A, and S1D). These changes mainly impacted the alpha, beta and, in part, also the gamma and delta variable genes (Figures 1G and 1H). *TRAV9-1*, *TRBV16,* and *TRBV11-3* in the lung and *TRAV9-2*, *TRAV41*, *TRAV22,* and *TRBV29-1* in the kidney were among the genes most downregulated (Figures 1G and 1H). When analyzing TCR alpha, beta, gamma, and delta constant genes (see Table S3), only *TRGC1* was significantly downregulated in COVID-19 lung when compared with control (Figure 1G); no significant changes were observed in TCR constant genes in COVID-19 kidney (Figure 1H).

When analyzing PBMC samples (Figure 2A), we noted substantial changes in the gene expression makeup of moderate and severe COVID-19 cases, when compared with convalescents and healthy controls (Figure 2B). Signature score analysis indicated that, compared to healthy controls, PBMCs obtained from severe patients showed marked alterations (i.e. $\geq$ 50% genes, for which the p value was $\leq 10^{-3}$ when compared with healthy control samples) in memory cell markers and Myc targets (see Figure S3A). *CCR7*, which was previously reported being upregulated in $CD4^+$ T-cells from children with multisystem inflammatory syndrome associated with SARS-CoV-2 (Carter et al., 2020), and the apoptotic markers *FASLG* and *TP53* were among the most significantly downregulated genes in these pathways (Figure 2C). Although at a rate lower than 50%, TCR alpha, beta, and, in part, gamma, and delta variable genes were downregulated in PBMC samples obtained from severe COVID-19 patients (Figure 2D). Signature score analysis on PBMCs obtained from moderate and convalescent cases indicated less marked changes in gene pathways in these two groups of subjects (see Figures S3B and S3C). When analyzing TCR alpha, beta, gamma, and delta constant genes, *TRAC*, *TRBC1/2,* and *TRDC* were significantly downregulated in PBMCs from severe COVID-19 patients when compared with control samples (Figure 2D).

The frequency of CD4 and CD8 cells positive for TCR V alpha 2 and TCR V beta 3.1 – two of the TCR variable genes that also underwent profound changes and for which detection using fluorochrome conjugated monoclonal antibodies was available – was determined by flow cytometry (Figures 2E, 2F, and S4A–S4D). There was a significant decrease in the frequency of CD4 cells positive for TCR V alpha 2 or TCR V beta 3.1 in severe COVID-19 patients, when compared with controls (Figures 2E, 2F, S4A, and S4C). The frequency of $CD4^+$ TCR V alpha 2^+ cells was also decreased in moderate COVID-19 patients and convalescents when compared with controls (Figures 2E and S4A). When considering CD8 cells, we noted decreased $CD8^+$ TCR V alpha 2^+ cell frequencies in severe COVID-19, when compared with moderate

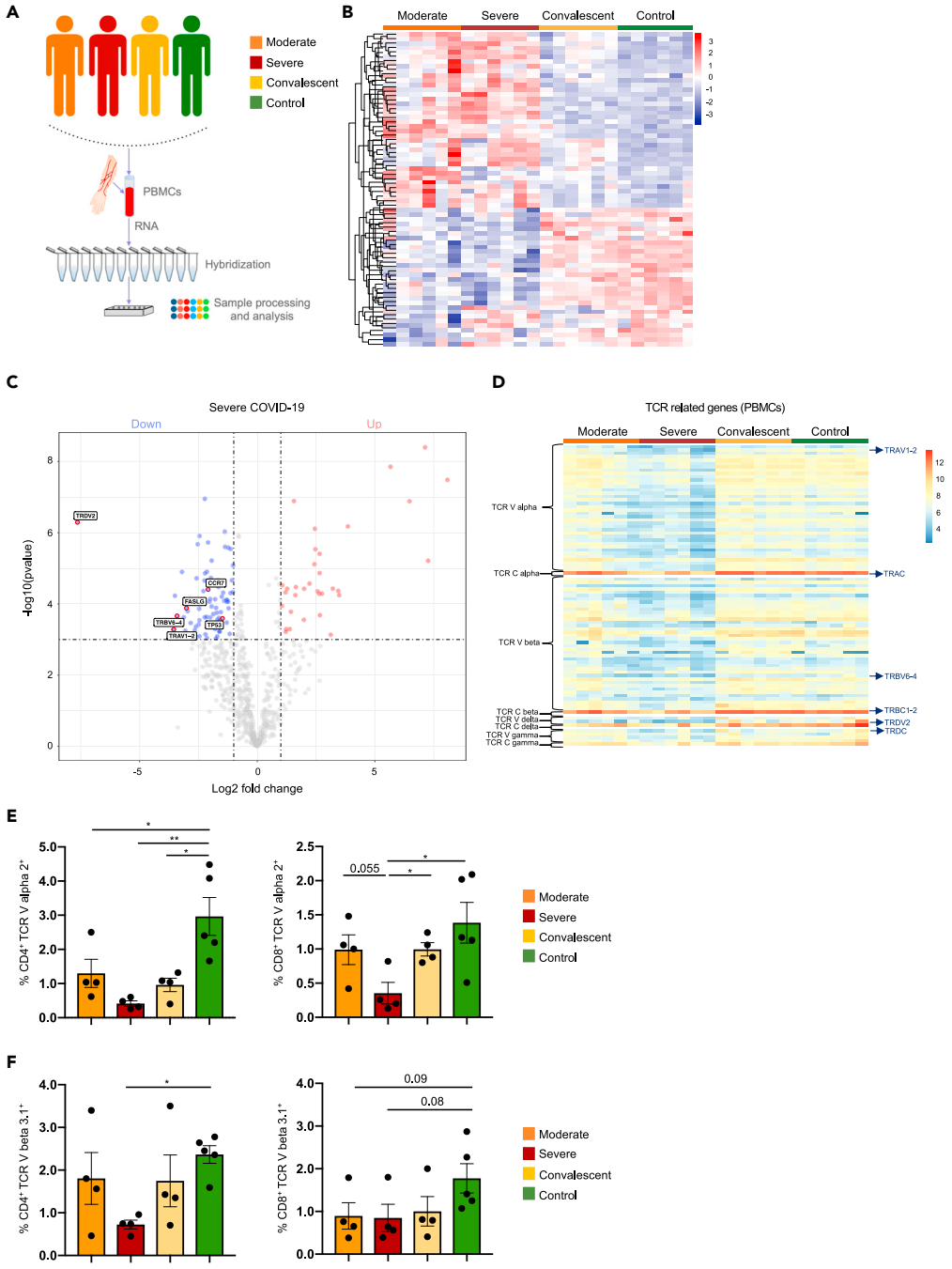

Figure 2. Limited TCR repertoire in PBMCs of severe COVID-19 patients

(A) Peripheral blood mononuclear cells (PBMCs) were obtained from severe (n = 6), moderate (n = 6) and convalescent (n = 6) COVID-19 patients and from healthy controls (n = 6). Total RNA was extracted and subjected to hybridization prior to NanoString processing and profiling.

(B) Heatmap showing differentially expressed genes (DEGs) included in the nCounter CAR-T Characterization Panel in PBMCs from moderate, severe and convalescent COVID-19 cases compared with controls. Upregulated and downregulated genes are shown in red and blue, respectively. DEGs were defined based on p value $\leq 10^{-3}$ (false discovery rate <0.05 in all cases).

(C) Volcano plot showing down- and upregulated genes in severe COVID-19 patients compared with controls. X and Y axes correspond to fold change and p value, respectively. Downregulated and upregulated genes are shown in blue and red. The most significantly downregulated genes are indicated.

Figure 2. *Continued*

(D) Heatmap representing TCR variable and constant alpha, beta, gamma, and delta genes in PBMCs obtained from moderate (n = 6), severe (n = 6), and convalescent (n = 6) COVID-19 patients and from healthy controls (n = 6). Data represented in the heatmap refer to gene expression normalized to the housekeeping genes included in the nCounter CAR-T genes. All samples subjected to NanoString analysis were run in triplicate and experiments performed independently three times.

(E and F) Frequency of $CD4^+$ V alpha 2^+, $CD8^+$ V alpha 2^+, $CD4^+$ V beta 3.1^+ and $CD8^+$ V beta 3.1^+ cells was determined by flow cytometry. Mean ± SEM frequency of (E) $CD4^+$ V alpha 2^+ and $CD8^+$ V alpha 2^+, and of (F) $CD4^+$ V beta 3.1^+ and $CD8^+$ V beta 3.1^+ cells in moderate (n = 4), severe (n = 4), convalescent (n = 4) COVID-19 patients and healthy controls (n = 5) is shown. *$p \leq 0.05$ and **$p \leq 0.01$ using one-way ANOVA followed by Tukey's multiple comparisons test. See also Figures S3 and S4.

COVID-19 cases, convalescents, and healthy individuals (Figures 2E and S4B). The frequency of $CD8^+$ TCR V beta 3.1^+ cells in severe and moderate COVID-19 patients was lower than that in healthy controls (Figures 2F and S4D); this decrease trended to significance in both cases (Figure 2F).

Upregulation of ENTPD1/CD39 in severe COVID-19

Alterations of purinergic signaling were previously reported in the context of viral infections (Gupta et al., 2015; Ravimohan et al., 2017) and found to be associated with worse disease outcome (Ravimohan et al., 2017). One of the key mediators of the purinergic pathway is ENTPD1/CD39, an ectonucleotidase that scavenges pro-inflammatory ATP and ADP into AMP, subsequently converted into immunosuppressive adenosine by NT5E/CD73, the ectoenzyme that works in tandem with CD39. *ENTPD1* was one of the most highly upregulated genes within the Treg pathway in the lung, liver, and spleen of COVID-19 patients, when compared with controls (Figures 3A and 3B). In these organs, CD39 was elevated not only at the RNA (Figure 3B) but also at the protein level, as indicated by immunohistochemistry staining (Figure 3C).

When analyzing PBMC samples, severe COVID-19 patients had higher levels of *ENTPD1*, when compared with moderate patients, convalescents, and healthy controls (Figure S5A); this finding being confirmed also by qPCR analysis, performed on PBMCs from a larger cohort of COVID-19 patients (Figure 3D). Importantly, when considering moderate and severe patients, *ENTPD1* mRNA levels were positively correlated with markers of vasculopathy like D-Dimer and prothrombin time (Figures 3E and 3F) and with length of stay in hospital and intensive care unit (Figures 3G and 3H).

We next subdivided COVID-19 patients into low and high *ENTPD1* expressing groups, based on the median value obtained after pooling the *ENTPD1* gene expression levels of severe and convalescent cases (median *ENTPD1* levels: 9.9, range: 9.43–10.77). We noted that high *ENTPD1* was associated with low expression of *TRGC1*, *CCR7*, and *CCR4* (Figures 4A and S6A), decreased levels of which have been also linked with impaired Treg suppression and exacerbation of inflammation in other infectious disease contexts (Bertolini et al., 2018); and with high levels of IL-6 (Figures 4A and S6A), a cytokine involved in CD39 induction via signal transducer and activator of transcription-3 (STAT-3) (Chalmin et al., 2012), IFNA1, and IL-33 (Figures 4A and S6A), known to be linked with poor COVID-19 outcome (Burke et al., 2020).

Gene set enrichment analysis (GSEA), where genes of the nCounter CAR-T Characterization panel were ranked based on *ENTPD1* expression levels of severe and convalescent cases, indicated that the high *ENTPD1*-expressing group mainly displayed enrichment in genes associated with chemokine and interleukin signaling pathways (Figures 4B and S6B), whereas the low *ENTPD1*-expressing group was inversely associated with TCR repertoire and interactions with non-lymphoid cell pathway (Figures 4B and S6B). Further analysis conducted to detect potential interactions between *ENTPD1/CD39* and other protein-coding genes included in the nCounter CAR-T panel and identified links with IL-6 and CCR7 that further corroborate the functional associations with these two molecules (Figure 4C).

Additional GSEA where the nCounter CAR-T genes were ranked based on the expression levels of *IL-6* and *IL-33* in the same groups of subjects, indicated that the high *IL-6* and *IL-33*-expressing group (median *IL-6*: 4.8, range: 3.1–6.9; median *IL-33*: median 4.55, range: 3.6–6.1) displayed enrichment in genes associated with chemokine and interleukin signaling (Figures S7A and S7B); whereas the low *IL-6* and *IL-33*-expressing group displayed an inverse association with genes related to the TCR repertoire (Figures S7A and S7B). nCAR-T gene ranking based on the expression levels of *CCR7* (median: 8.8, range: 6.1–9.9) revealed that

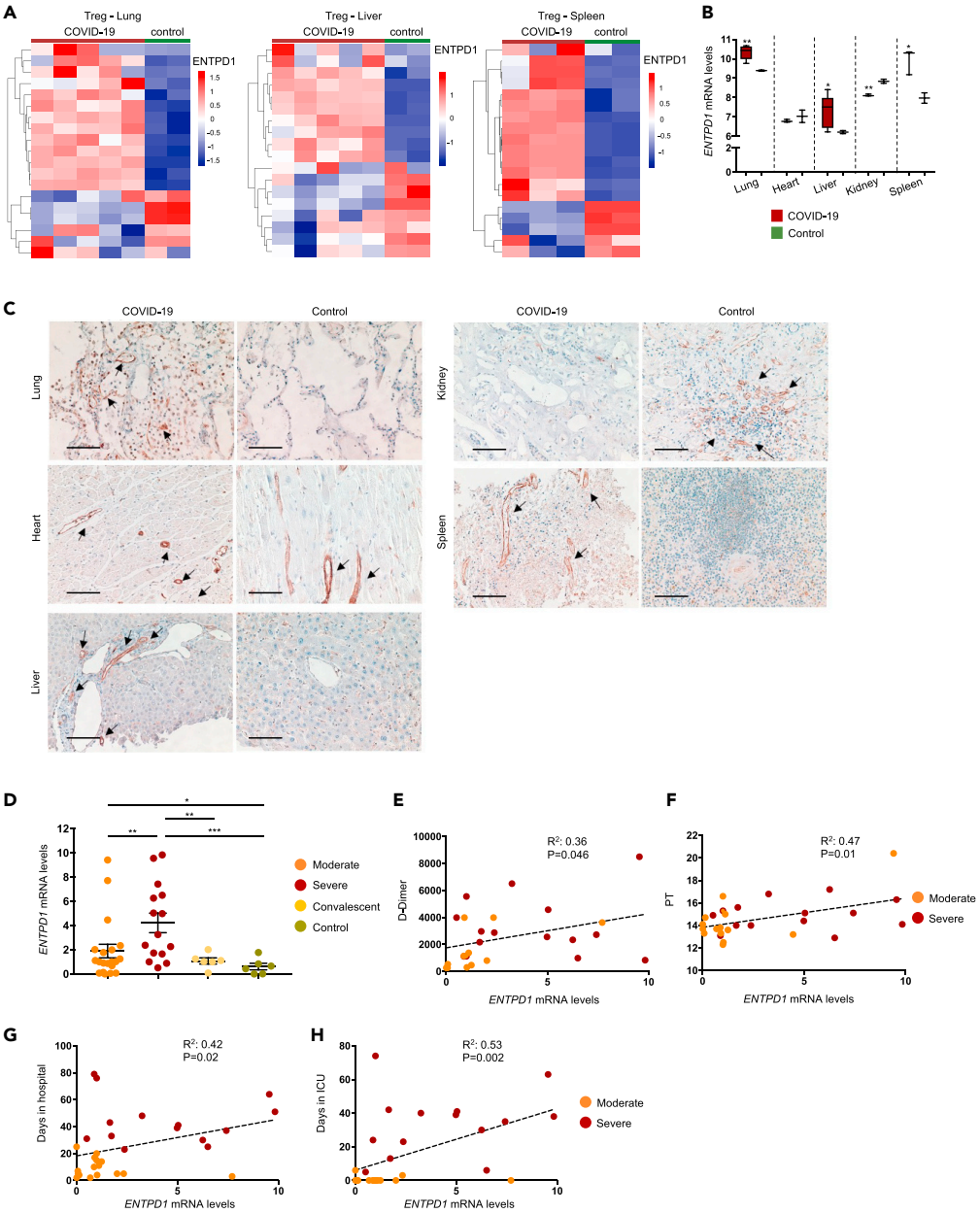

Figure 3. Increased *ENTPD1* levels in lung, liver, spleen, and PBMCs from severe COVID-19 patients

(A) Heatmaps representing the Treg gene set in lung, liver, and spleen of COVID-19 patients, compared with controls. Upregulated and downregulated genes are shown in red and blue.

(B) Box plots showing the median *ENTPD1* levels in biopsies from autoptic lung, heart, liver, kidney and spleen of COVID-19 patients (lung n = 5, liver n = 5, spleen n = 3) and controls (n = 2 for all organs). Results were obtained by NanoString. *p $\leq$ 0.05; **p $\leq$ 0.01 using two-sided unpaired t test. Samples were run in triplicate and experiments performed independently three times.

(C) Expression of CD39 was tested in paraffin embedded sections obtained from biopsies of autoptic COVID-19 and control lung, heart, liver, kidney and spleen. Immunohistochemistry staining is shown from one COVID-19 patient and one control. Arrows indicate positively stained cells (magnification 20 x, scale bar 100 μM). A representative of three independent staining is shown.

(D) *ENTPD1* mRNA levels in PBMCs were determined by qPCR in moderate (n = 20), severe (n = 15), convalescent (n = 6) COVID-19 cases and in healthy controls (n = 6). Mean ± SEM is shown. *p $\leq$ 0.05, **p $\leq$ 0.01 and ***p $\leq$ 0.001 using one-way ANOVA followed by Tukey's multiple comparisons test. Samples were run in triplicate and experiments performed independently three times.

Figure 3. *Continued*
(E–H) Correlation between *ENTPD1* mRNA levels and (E) D-Dimer, (F) prothrombin time (PT), length of stay in (G) hospital, and (H) intensive care unit (ICU) in moderate and severe patients. Coefficients associated with significant ($p \leq 0.05$) correlations are indicated. See also Figure S5.

the high *CCR7*-expressing group was enriched in genes related to the TCR repertoire and interactions with non-lymphoid cell pathway (Figure S7C), whereas the low *CCR7*-expressing group showed an inverse association with genes of the chemokine and interleukin signaling pathways (Figure S7C).

Aberrant ENTPD1/CD39 regulation in late-stage COVID-19

Others and we have previously shown that ENTPD1/CD39 has a pivotal role in the maintenance of immune homeostasis, being regulated at the genetic level by polymorphisms in the promoter region that are associated with low mRNA levels (Friedman et al., 2009; Rissiek et al., 2015; Timperi et al., 2016; Adhikary et al., 2020). ENTPD1/CD39 can be also regulated at the transcriptional level by transcription factors such as the aryl hydrocarbon receptor (AHR), a toxin mediator that modulates adaptive immunity (Quintana et al., 2008; Veldhoen et al., 2008), which has been recently involved in SARS-CoV-2 pathology (Giovannoni et al., 2021); STAT-3 that induces CD39 in Th17 cells (Chalmin et al., 2012) and indirectly by hypoxia-inducible-factor-1-alpha (HIF-1α) via Sp1 (Eltzschig et al., 2009). In PBMCs, we detected an increase in the levels of both *STAT-3* and *HIF-1α*, in severe COVID-19 patients, when compared with healthy controls and convalescents (Figures 4D and 4E), while no differences were noted in the levels of AHR among different groups of patients (Figure 4F).

We have recently shown that ENTPD1/CD39 can be also regulated by an endogenous antisense RNA, which is present in multiple splice variants in antisense position to *ENTPD1* at 10q24.1 (Harshe et al., 2020). qPCR analysis indicated downregulation in the levels of *CD39-AS* RNA in severe COVID-19 patients, when compared with convalescents and controls (Figure 4G). Levels of *CD39-AS* RNA in moderate COVID-19 patients were also lower than in controls (Figure 4G).

DISCUSSION

Our data show that in severe COVID-19 patients there are alterations in the expression of TCR variable genes along with aberrant regulation of *ENTPD1/CD39*, the latter resulting in the upregulation of this ectoenzyme at both systemic and organ levels. A marked decrease in the expression of alpha and beta variable genes was noted when analyzing samples obtained from lung, kidney, and PBMCs of severe COVID-19 patients, as compared with other COVID-19 subgroups and controls. Changes in the TCR constant genes were less evident, suggesting a more prominent impact on the TCR variable region. Although derived from a relatively small number of samples, the flow cytometry data showing decrease in the frequency of CD4 and CD8 cells positive for TCR V alpha 2 and of CD4 cells positive for TCR V beta 3.1 in severe COVID-19 patients corroborate the findings obtained at the gene level. Our data indicate that alterations in TCR repertoire are present in both CD4 and CD8 cell subsets, although studies on larger patients' cohorts are needed to confirm these data.

Decreases in TCR repertoire have been previously linked to immune exhaustion, as in severe HIV and AIDS (Hernandez et al., 2018), early septic shock (Tomino et al., 2017), and tuberculosis (Luo et al., 2012). These changes may lead to inadequate adaptive immune function as a result of limited capability of antigen recognition by T lymphocytes. Further studies at the single-cell level would aid determining which specific T helper/cytotoxic cell subset undergoes downregulation of TCR-related genes in different stages of COVID-19 and whether these subsets are phenotypically and functionally exhausted.

The increases in ENTPD1/CD39 noted in the lung, liver, and spleen, and PBMCs of severe COVID-19 cases indicate likewise associations with disease progression and severity. Such linkages have been previously reported in the context of HIV infection, where high levels of CD39 in CD8 T-cells were associated with immune exhaustion (Gupta et al., 2015) and early mortality (Ravimohan et al., 2017). Increases in the expression of CD39 in peripheral blood-derived CD4 and CD8 cells were reported earlier in hospitalized COVID-19 patients, and further associated with increases in CD38, PD-1, and HLA-DR levels, as determined by high-dimensional flow cytometry analysis (Mathew et al., 2020). However, whether these cellular changes were present in end-organs (lung, kidney) was not tested in earlier studies. Our data indicating a positive correlation between *ENTPD1* mRNA levels

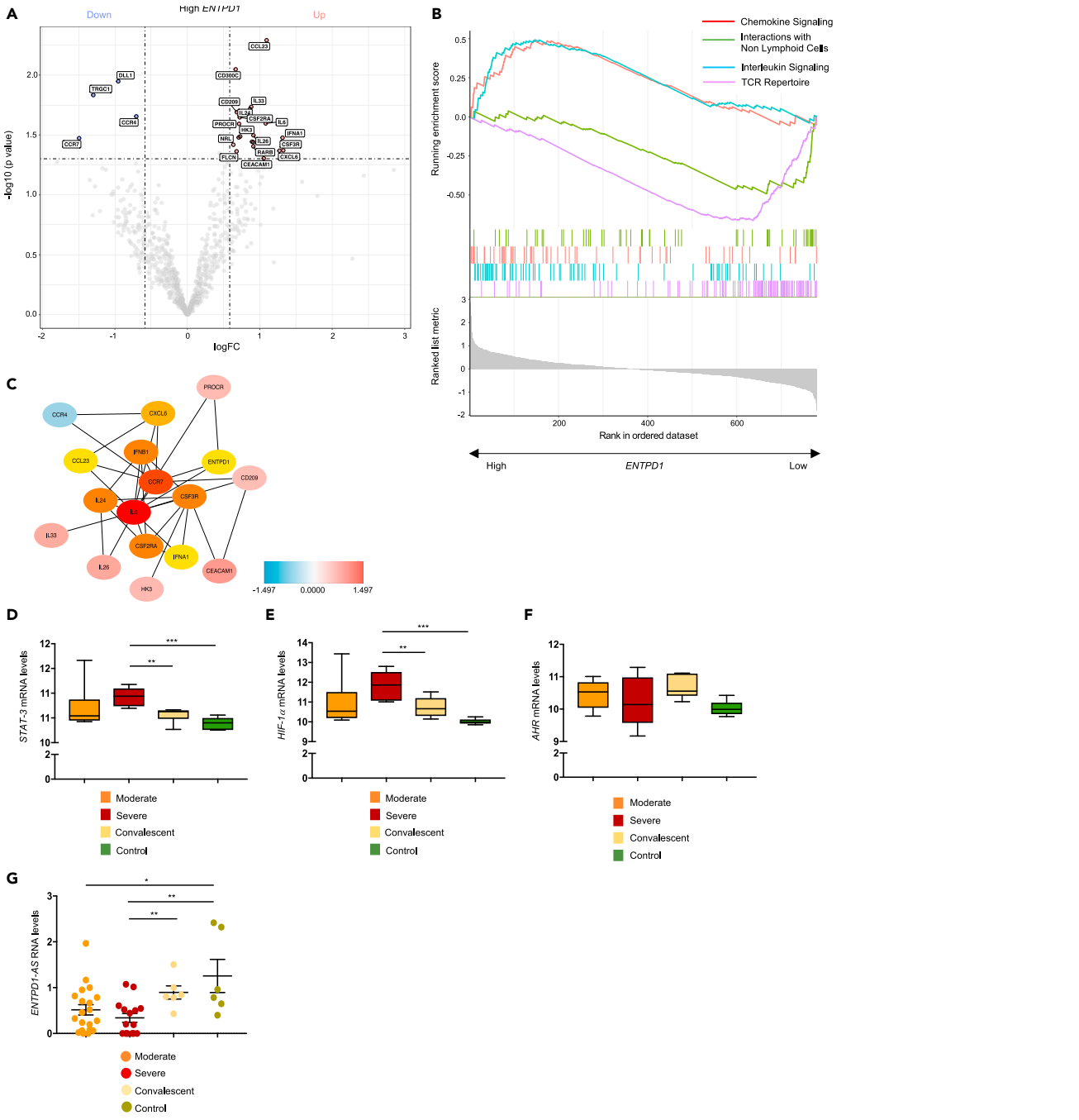

Figure 4. *ENTPD1* is aberrantly regulated in severe COVID-19 patients

(A) Volcano plot showing down- and upregulated genes within the high *ENTPD1* expressing group. High and low *ENTPD1* expression was defined based on the median value (median *ENTPD1* levels: 9.9, range: 9.43–10.77 obtained after pooling the *ENTPD1* gene expression levels of severe and convalescent cases. nCounter CAR-T genes were then subdivided based on *ENTPD1* levels and subsequently associated with high or low *ENTPD1* expression. X and Y axes correspond to fold change and p value respectively. Downregulated and upregulated genes are shown in blue and red. The most significantly downregulated and upregulated genes are indicated.

(B) Gene set enrichment analysis (GSEA) showing the gene pathways associated with high and low *ENTPD1* expression levels (p value < 0.05 and false discovery rate q value < 0.05). High and low *ENTPD1* expression was defined based on the median value obtained after pooling the *ENTPD1* gene expression levels of severe and convalescent cases. nCounter CAR-T genes were then subdivided based on *ENTPD1* levels and associated with high or low *ENTPD1* expression. Lines

Figure 4. *Continued*
represent individual gene sets. Upregulated genes are located on the left, while downregulated genes are located on the right of the plot.
(C) PPI network between *ENTPD1/CD39* and other protein-coding genes included in the nCounter CAR-T characterization panel was derived by STRING (threshold value of median confidence of 0.4).
(D–F) Box plots showing the median (D) *STAT-3*, (E) *HIF-1α*, and (F) *AHR* mRNA levels in PBMCs from moderate (n = 6), severe (n = 6) and convalescent (n = 6) COVID-19 patients and healthy controls (n = 6). Data were obtained by NanoString analysis. **p ≤ 0.01 and ***p ≤ 0.001 using one-way ANOVA followed by Tukey's multiple comparisons test. Samples were run in triplicate and experiments performed independently three times.
(G) Levels of *ENTPD1-AS* RNA were tested by qPCR in moderate (n = 20), severe (n = 15), convalescent (n = 6) COVID-19 cases and in healthy controls (n = 6). Mean ± SEM *ENTPD1-AS* RNA is shown. *p ≤ 0.05, **p ≤ 0.01 and ***p ≤ 0.001 using one-way ANOVA followed by Tukey's multiple comparisons test. Samples were run in triplicate and experiments performed independently three times. See also Figures S6 and S7.

with D-dimer, prothrombin time, and other clinical parameters like the length of stay in hospital or intensive care unit suggest a role for CD39 as a prognostic marker for disease severity.

Our GSEA results showing a negative association between high CD39 levels and limited TCR repertoire might suggest that the overly suppressive microenvironment, derived from high CD39 and adenosine levels, might predispose to further inflammatory insults and immune compromise. Future studies should be directed at testing whether increase in CD39 expression is indeed associated with increased ectoenzymatic activity and, consequently, heightened adenosine generation.

Our data suggest important functional associations between ENTPD1/CD39 with IL-6, IL-33, and CCR7. In this regard, GSEA studies show that high (or low) expression of these molecules was associated with the chemokine and interleukin signaling gene sets and the TCR repertoire, postulating a role for CD39, IL-6, IL-33, and CCR7 in the modulation of these pathways in the setting of COVID-19.

As shown by our findings, upregulation of ENTPD1/CD39 in late-stage COVID-19 could be associated with aberrant regulation of this ectoenzyme, as indicated by heightened levels of STAT-3 and HIF-1α, which contribute to CD39 modulation at the transcriptional level (Chalmin et al., 2012; Xie et al., 2018; Mascanfroni et al., 2015). Aberrant CD39 regulation in COVID-19 might also derive from decreased levels of *CD39-AS* RNA, as we have recently reported (Harshe et al., 2020). This endogenous antisense RNA regulates *ENTPD1* expression and was previously found elevated in the peripheral blood and lamina propria-derived Tregs and Th17 cells of Crohn's disease patients (Harshe et al., 2020). It remains to be determined whether high levels of *ENTPD1* in severe COVID-19 subjects are also associated with the possession of GG alleles at rs10748643, as others and we have previously shown (Friedman et al., 2009; Rissiek et al., 2015; Timperi et al., 2016; Adhikary et al., 2020). Further investigations in larger cohorts of COVID-19 patients and controls are needed to address this important point.

It is unclear whether T cells with specificity for viral epitopes do preferentially express high levels of CD39. Previous work in the context of cancer has shown that tumor-infiltrating, non-specific "bystander" CD8 T-cells preferentially recognize viral epitopes (e.g. influenza and cytomegalovirus) instead of tumor antigens and lack CD39 expression (Simoni et al., 2018). Based on this earlier study, it is unlikely that T cells recognizing COVID-19 epitopes are those expressing high levels of CD39, although additional work at the functional and/or single-cell level might help elucidating this.

In conclusion, we have shown that perturbations in T cell immunity in COVID-19 can be linked to limitations in the TCR repertoire, systemically with blood cells and locally, at the organ level. We also note aberrant elevations of ENTPD1/CD39, possibly associated with enhanced expression of CD39-related transcription factors along with decreases in the levels of CD39 endogenous antisense. These changes might contribute to a purinergic imbalance that perpetuates immunosuppression, resulting in metabolic changes and T cell dysfunction. Strategies that interfere with these purinergic alterations as in the case of antibodies to CD39 might be beneficial in preventing COVID-19 progression or in stabilizing those patients with severe disease.

Limitations of the study

We acknowledge that the analysis of a small number of biopsies, obtained at autopsy from non-COVID-19 controls, is a limitation of our study and that a larger number of such biopsies is needed for a complete

validation of our findings. However, due to the clear time constraints related to the ongoing COVID-19 pandemic and the clinical and logistical limitations in obtaining additional controls at autopsy, we have preferred making these earlier investigations available to the scientific community now.

STAR★METHODS

Detailed methods are provided in the online version of this paper and include the following:

- KEY RESOURCES TABLE
- RESOURCE AVAILABILITY
  - Lead contact
  - Materials availability
  - Data and software availability
- EXPERIMENTAL MODEL AND SUBJECT DETAILS
- METHODS DETAILS
  - Sample preparation
  - RNA extraction and NanoString transcriptomic profiling
  - qPCR
  - Immunohistochemistry
  - Flow cytometry
- QUANTIFICATION AND STATISTICAL ANALYSIS

SUPPLEMENTAL INFORMATION

Supplemental information can be found online at https://doi.org/10.1016/j.isci.2021.103205.

ACKNOWLEDGMENTS

Grant support: This work has been supported by the National Institutes of Health (R01 DK108894 and R01 DK124408 to M.S.L.); Seed Grant Award (Department of Anesthesia, Critical Care & Pain Medicine to M.S.L.); the Department of Defense Award W81XWH-16-0464 (to S.C.R.).

AUTHOR CONTRIBUTIONS

Acquisition of data, analysis and interpretation of data, and drafting of the manuscript, N.W., M.V., A.K.; acquisition and analysis of data, J.J.G.; acquisition of data, E.C., Z.J.M.H., and A.W.; analysis and interpretation of data, C.D., E.M., and K.G.; critical revision of the manuscript, J.L.H., S.S., S.C.R., and M.S.L.; writing of the manuscript, M.S.L; obtained funding, M.S.L. and S.C.R.

DECLARATION OF INTERESTS

C.D. and K.G. are employees and shareholders of NanoString Technologies, Inc. E.M.M. was an employee and shareholder of NanoString Technologies, Inc at the time of study.

Received: June 11, 2021
Revised: September 6, 2021
Accepted: September 28, 2021
Published: October 22, 2021

REFERENCES

Adhikary, S.R., Cuthbertson, P., Turner, R.J., Sluyter, R., and Watson, D. (2020). A single-nucleotide polymorphism in the human ENTPD1 gene encoding CD39 is associated with worsened graft-versus-host disease in a humanized mouse model. Immunol. Cell Biol. *98*, 397–410.

Bertolini, T.B., Pineros, A.R., Prado, R.Q., Gembre, A.F., Ramalho, L.N.Z., Alves-Filho, J.C., and Bonato, V.L.D. (2018). CCR4-dependent reduction in the number and suppressor function of CD4(+)Foxp3(+) cells augments IFN-gamma-mediated pulmonary inflammation and aggravates tuberculosis pathogenesis. Cell Death Dis. *10*, 11.

Burke, H., Freeman, A., Cellura, D.C., Stuart, B.L., Brendish, N.J., Poole, S., Borca, F., Phan, H.T.T., Sheard, N., Williams, S., et al. (2020). Inflammatory phenotyping predicts clinical outcome in COVID-19. Respir. Res. *21*, 245.

Carter, M.J., Fish, M., Jennings, A., Doores, K.J., Wellman, P., Seow, J., Acors, S., Graham, C., Timms, E., Kenny, J., et al. (2020). Peripheral immunophenotypes in children with multisystem inflammatory syndrome associated with SARS-CoV-2 infection. Nat. Med. *26*, 1701–1707.

Chalmin, F., Mignot, G., Bruchard, M., Chevriaux, A., Vegran, F., Hichami, A., Ladoire, S., Derangere, V., Vincent, J., Masson, D., et al. (2012). Stat3 and Gfi-1 transcription factors control Th17 cell immunosuppressive activity via the regulation of ectonucleotidase expression. Immunity *36*, 362–373.

Eltzschig, H.K., Kohler, D., Eckle, T., Kong, T., Robson, S.C., and Colgan, S.P. (2009). Central role of Sp1-regulated CD39 in hypoxia/ischemia protection. Blood *113*, 224–232.

Friedman, D.J., Kunzli, B.M., Yi, A.R., Sevigny, J., Berberat, P.O., Enjyoji, K., Csizmadia, E., Friess, H., and Robson, S.C. (2009). From the Cover: CD39 deletion exacerbates experimental murine colitis and human polymorphisms increase susceptibility to inflammatory bowel disease. Proc. Natl. Acad. Sci. U. S. A. *106*, 16788–16793.

Giovannoni, F., Li, Z., Remes-Lenicov, F., Davola, M.E., Elizalde, M., Paletta, A., Ashkar, A.A., Mossman, K.L., Dugour, A.V., Figueroa, J.M., et al. (2021). AHR signaling is induced by infection with coronaviruses. Nat. Commun. *12*, 5148.

Gupta, P.K., Godec, J., Wolski, D., Adland, E., Yates, K., Pauken, K.E., Cosgrove, C., Ledderose, C., Junger, W.G., Robson, S.C., et al. (2015). CD39 expression identifies terminally exhausted CD8+ T cells. Plos Pathog. *11*, e1005177.

Harshe, R.P., XIE, A., Vuerich, M., Frank, L.A., Gromova, B., Zhang, H., Robles, R.J., Mukherjee, S., Csizmadia, E., Kokkotou, E., et al. (2020). Endogenous antisense RNA curbs CD39 expression in Crohn's disease. Nat. Commun. *11*, 5894.

Hernandez, D.M., Valderrama, S., Gualtero, S., Hernandez, C., Lopez, M., Herrera, M.V., Solano, J., Fiorentino, S., and Quijano, S. (2018). Loss of T-cell multifunctionality and TCR-Vbeta repertoire against Epstein-Barr virus is associated with worse prognosis and clinical parameters in HIV(+) patients. Front. Immunol. *9*, 2291.

Kusnadi, A., Ramirez-Suastegui, C., Fajardo, V., Chee, S.J., Meckiff, B.J., Simon, H., Pelosi, E., Seumois, G., AY, F., Vijayanand, P., and Ottensmeier, C.H. (2021). Severely ill COVID-19 patients display impaired exhaustion features in SARS-CoV-2-reactive CD8(+) T cells. Sci. Immunol. *6*, eabe4782.

Laing, A.G., Lorenc, A., del Molino del barrio, I., Das, A., Fish, M., Monin, L., Munoz-Ruiz, M., Mckenzie, D.R., Hayday, T.S., Francos-Quijorna, I., et al. (2020). A dynamic COVID-19 immune signature includes associations with poor prognosis. Nat. Med. *26*, 1623–1635.

Liberal, R., Grant, C.R., Ma, Y., Csizmadia, E., Jiang, Z.G., Heneghan, M.A., Yee, E.U., Mieli-Vergani, G., Vergani, D., Robson, S.C., and Longhi, M.S. (2016). CD39 mediated regulation of Th17-cell effector function is impaired in juvenile autoimmune liver disease. J. Autoimmun. *72*, 102–112.

Luo, W., Su, J., Zhang, X.B., Yang, Z., Zhou, M.Q., Jiang, Z.M., Hao, P.P., Liu, S.D., Wen, Q., Jin, Q., and Ma, L. (2012). Limited T cell receptor repertoire diversity in tuberculosis patients correlates with clinical severity. PLoS One *7*, e48117.

Mascanfroni, I.D., Takenaka, M.C., Yeste, A., Patel, B., Wu, Y., Kenison, J.E., Siddiqui, S., Basso, A.S., Otterbein, L.E., Pardoll, D.M., et al. (2015). Metabolic control of type 1 regulatory T cell differentiation by AHR and HIF1-alpha. Nat. Med. *21*, 638–646.

Mathew, D., Giles, J.R., Baxter, A.E., Oldridge, D.A., Greenplate, A.R., Wu, J.E., Alanio, C., Kuri-Cervantes, L., Pampena, M.B., D'Andrea, K., et al. (2020). Deep immune profiling of COVID-19 patients reveals distinct immunotypes with therapeutic implications. Science *369*, eabc8511.

Orologas-Stavrou, N., Politou, M., Rousakis, P., Kostopoulos, I.V., Ntanasis-Stathopoulos, I., Jahaj, E., Tsiligkeridou, E., Gavriatopoulou, M., Kastritis, E., Kotanidou, A., et al. (2020). Peripheral blood immune profiling of convalescent plasma donors reveals alterations in specific immune subpopulations even at 2 Months post SARS-CoV-2 infection. Viruses *13*, 26.

Peng, Y., Mentzer, A.J., Liu, G., Yao, X., Yin, Z., Dong, D., Dejnirattisai, W., Rostron, T., Supasa, P., Liu, C., et al. (2020). Broad and strong memory CD4(+) and CD8(+) T cells induced by SARS-CoV-2 in UK convalescent individuals following COVID-19. Nat. Immunol. *21*, 1336–1345.

Quintana, F.J., Basso, A.S., Iglesias, A.H., Korn, T., Farez, M.F., Bettelli, E., Caccamo, M., Oukka, M., and Weiner, H.L. (2008). Control of T(reg) and T(H) 17 cell differentiation by the aryl hydrocarbon receptor. Nature *453*, 65–71.

Ravimohan, S., tamuhla, N., Nfanyana, K., Ni, H., Steenhoff, A.P., Gross, R., Weissman, D., and Bisson, G.P. (2017). Elevated pre-antiretroviral therapy CD39+CD8+ T cell frequency is associated with early mortality in advanced human immunodeficiency virus/tuberculosis co-infection. Clin. Infect. Dis. *64*, 1453–1456.

Rissiek, A., Baumann, I., Cuapio, A., Mautner, A., Kolster, M., Arck, P.C., Dodge-Khatami, A., Mittrucker, H.W., Koch-Nolte, F., Haag, F., and Tolosa, E. (2015). The expression of CD39 on regulatory T cells is genetically driven and further upregulated at sites of inflammation. J. Autoimmun. *58*, 12–20.

Ritchie, M.E., Phipson, B., Wu, D., Hu, Y., Law, C.W., Shi, W., and Smyth, G.K. (2015). Limma powers differential expression analyses for RNA-sequencing and microarray studies. Nucleic Acids Res. *43*, e47.

Sette, A., and Crotty, S. (2021). Adaptive immunity to SARS-CoV-2 and COVID-19. Cell *184*, 861–880.

Shannon, P., Markiel, A., Ozier, O., Baliga, N.S., Wang, J.T., Ramage, D., Amin, N., Schwikowski, B., and Ideker, T. (2003). Cytoscape: a software environment for integrated models of biomolecular interaction networks. Genome Res. *13*, 2498–2504.

Simoni, Y., Becht, E., Fehlings, M., Loh, C.Y., Koo, S.L., Teng, K.W.W., Yeong, J.P.S., Nahar, R., Zhang, T., Kared, H., et al. (2018). Bystander CD8(+) T cells are abundant and phenotypically distinct in human tumour infiltrates. Nature *557*, 575–579.

Timperi, E., Folgori, L., Amodio, D., de Luca, M., Chiurchiu, S., Piconese, S., di Cesare, S., Pacella, I., Martire, C., Bonatti, G., et al. (2016). Expansion of activated regulatory T cells inversely correlates with clinical severity in septic neonates. J. Allergy Clin. Immunol. *137*, 1617–1620.e6.

Tomino, A., Tsuda, M., Aoki, R., Kajita, Y., Hashiba, M., Terajima, T., Kano, H., and Takeyama, N. (2017). Increased PD-1 expression and altered T cell repertoire diversity predict mortality in patients with septic shock: a preliminary study. PLoS One *12*, e0169653.

Veldhoen, M., Hirota, K., Westendorf, A.M., Buer, J., Dumoutier, L., Renauld, J.C., and Stockinger, B. (2008). The aryl hydrocarbon receptor links TH17-cell-mediated autoimmunity to environmental toxins. Nature *453*, 106–109.

Vuerich, M., Harshe, R., Frank, L.A., Mukherjee, S., Gromova, B., Csizmadia, E., Nasser, I.A.M., Ma, Y., Bonder, A., patwardhan, V., et al. (2021). Altered aryl-hydrocarbon-receptor signalling affects regulatory and effector cell immunity in autoimmune hepatitis. J. Hepatol. *74*, 48–57.

Wang, F., Hou, H., Luo, Y., Tang, G., Wu, S., Huang, M., Liu, W., Zhu, Y., Lin, Q., Mao, L., et al. (2020). The laboratory tests and host immunity of COVID-19 patients with different severity of illness. JCI Insight *5*, e137799.

Wilk, A.J., Rustagi, A., Zhao, N.Q., Roque, J., Martinez-Colon, G.J., Mckechnie, J.L., Ivison, G.T., Ranganath, T., Vergara, R., Hollis, T., et al. (2020). A single-cell atlas of the peripheral immune response in patients with severe COVID-19. Nat. Med. *26*, 1070–1076.

Xie, A., Robles, R.J., Mukherjee, S., Zhang, H., Feldbrugge, L., Csizmadia, E., Wu, Y., Enjyoji, K., Moss, A.C., Otterbein, L.E., et al. (2018). HIF-1alpha-induced xenobiotic transporters promote Th17 responses in Crohn's disease. J. Autoimmun. *94*, 122–133.

Yao, C., Bora, S.A., Parimon, T., Zaman, T., Friedman, O.A., Palatinus, J.A., Surapaneni, N.S., Matusov, Y.P., Cerzro Chiang, G., Kassar, A.G., et al. (2021). Cell-Type-specific immune dysregulation in severely ill COVID-19 patients. Cell Rep. *34*, 108590.

Yu, G., Wang, L.G., Han, Y., and He, Q.Y. (2012). clusterProfiler: an R package for comparing biological themes among gene clusters. OMICS *16*, 284–287.

Zhang, J.Y., Wang, X.M., Xing, X., Xu, Z., Zhang, C., Song, J.W., Fan, X., Xia, P., Fu, J.L., Wang, S.Y., et al. (2020). Single-cell landscape of immunological responses in patients with COVID-19. Nat. Immunol. *21*, 1107–1118.

Zhu, L., Yang, P., Zhao, Y., Zhuang, Z., Wang, Z., Song, R., Zhang, J., Liu, C., Gao, Q., Xu, Q., et al. (2020). Single-cell sequencing of peripheral mononuclear cells reveals distinct immune response landscapes of COVID-19 and influenza patients. Immunity *53*, 685–696.e3.

STAR★METHODS

KEY RESOURCES TABLE

REAGENT or RESOURCE	SOURCE	IDENTIFIER
Antibodies		
Rabbit polyclonal anti-human CD39	Sigma Aldrich	Cat. # HPA014067; RRID:AB_1848178
Goat anti-rabbit IgG antibody	Vector Laboratories	Cat. # BA-1000; RRID:AB_2313606
TCR V alpha 2 monoclonal antibody	Invitrogen	Cat. # TCR2663; RRID:AB_417093
TCR V beta 3.1 monoclonal antibody	Invitrogen	Cat. # TCR2740; RRID:AB_223625
PerCP/Cyanine 5.5 anti-human CD4	Biolegend	Cat. # 317428; RRID:AB_1186122
PE anti-human CD8	Biolegend	Cat. # 344706; RRID:AB_1953244
Brilliant Violet 785 anti-human CD3	Biolegend	Cat. # 317330; RRID:AB_2563507
Biological samples		
COVID-19 PBMC samples	Massachusetts General Hospital and Brigham's and Women's Hospital	https://www.massgeneral.org https://www.brighamandwomens.org
COVID-19 and non-COVID-19 FFPE samples	Beth Israel Deaconess Medical Center	https://www.bidmc.org
Healthy controls PBMC samples	Blood Donor Center at Boston Children's Hospital	https://www.childrenshospital.org/ways-to-help/donate-blood
Critical commercial assays		
RNeasy Mini kit (50)	Qiagen	Cat. # 74104
AllPrep DNA/RNA FFPE kit	Qiagen	Cat. # 80234
nCounter CAR-T Characterization Panel	NanoString	Cat. # XT-CSO-CART1-12
iScript cDNA synthesis kit	Bio-Rad Laboratories	Cat. # 1708891BUN
Oligonucleotides		
Human *CD39/ENTPD1* forward 5′ AGGTGCCTATGGCTGGATTAC 3′	Harshe et al. (2020)	NA
Human *CD39/ENTPD1* reverse 5′ CCAAAGCTCCAAAGGTTTCC 3′	Harshe et al. (2020)	NA
Human *CD39-AS* forward 5′ AATACTGTGACACTGACCACCAGG 3	Harshe et al. (2020)	NA
Human *CD39-AS* reverse 5′ TGAATCCACTCTGTCTCCTGCA 3′	Harshe et al. (2020)	NA
Human *β-actin* forward 5′ CTCTTCCAGCCTTCCTTCCT 3′	This paper	NA
Human *β-actin* reverse 5′ AGCACTGTGTTGGCGTACAG 3′	This paper	NA
Software and algorithms		
nSolver™ Analysis Software, 4.0	NanoString Technologies	https://www.nanostring.com/products/analysis-solutions/ncounter-advanced-analysis-software/
R software, 4.0.2	R	https://cran.r-project.org
pheatmap package	R environment	https://CRAN.R-project.org/package=pheatmap
limma package	Ritchie et al. (2015)	https://bioconductor.org/packages/release/bioc/html/limma.html
clusterProfiler package	Yu et al. (2012)	http://www.bioconductor.org/packages/release/bioc/html/clusterProfiler.html

(*Continued on next page*)

Continued

REAGENT or RESOURCE	SOURCE	IDENTIFIER
enrichplot package	Yu et al. (2012)	https://yulab-smu.top/biomedical-knowledge-mining-book/
Cytoscape software, 3.8.2	Shannon et al. (2003)	https://cytoscape.org/
FlowJo, 10	FlowJo	https://www.flowjo.com
QuantStudio Design & Analysis software, 1.5.1	Applied Biosystems	https://www.thermofisher.com/us/en/home/global/forms/life-science/quantstudio-3-5-software.html

RESOURCE AVAILABILITY

Lead contact

Further information and requests for resources and reagents should be directed to and will be fulfilled by the lead contact, Maria Serena Longhi (mlonghi@bidmc.harvard.edu).

Materials availability

This study did not generate new unique reagents.

Data and software availability

NanoString bulk transcriptomics data are provided in Table S4 and are available from Mendeley Data at https://doi.org/10.17632/mkmv3mgz86.1.

qPCR and all other data reported in this paper are available from the lead contact upon request.

This paper does not report original code.

Any additional information required to reanalyze the data reported in this paper is available from the lead contact upon request.

EXPERIMENTAL MODEL AND SUBJECT DETAILS

PBMC samples were obtained from a total of 45 COVID-19 patients recruited from Massachusetts General Hospital (n = 30) and Brigham and Women's Hospital (n = 15) as part of the Massachusetts Consortium on Pathogen Readiness initiative. All patients had laboratory confirmed COVID-19 (detected by nasopharyngeal or oropharyngeal swabs). Of these 45 patients, 20 had moderate disease while 15 had severe disease and 10 were convalescents. As per World Health Organization definition, severe cases were defined as those with clinical signs of pneumonia in association with one of the following signs: respiratory rate higher than 30 breaths/min, severe respiratory distress and SpO_2<93% on room air. In moderate and severe cases, PBMC samples were collected at the time of hospital admission. In the case of convalescents, PBMCs were obtained during recovery, 4–12 weeks after the onset of symptoms. PBMCs were also obtained from 10 healthy controls (6 males and 4 females; median age 39 years, range 26–55).

Ultrasound guided biopsies of autoptic lung, heart, kidney, liver and spleen were obtained from 5 COVID-19 patients (1 moderate, 4 severe) and 2 non-COVID-19 controls (one male, 65 year-old; one female 59 year-old). These were carried out in the Pathology Department, Beth Israel Deaconess Medical Center (BIDMC), Boston. In COVID-19 cases, death occurred as a result of COVID-19 related multi-organ failure; whereas in the non-COVID-19 controls death was due to brain fungal infection in one case and shock in the setting of acute on chronic liver failure from established, non-infectious liver cirrhosis, in the other. The histopathological findings in the organs of COVID-19 patients were representative of SARS-CoV-2-related injury and consistent with previous reports (Simoni et al., 2018). Demographic and clinical data of all COVID-19 patients recruited in the study are summarized in Table S2. The study received IRB approval (protocol # 2020P000675) by the Committee of Clinical Investigations, BIDMC. Written informed consent was obtained from all study participants prior to inclusion in the study.

METHODS DETAILS

Sample preparation

Peripheral blood samples were collected in ethylenediaminetetraacetic acid-anticoagulated tubes. PBMCs were obtained by density gradient centrifugation on Ficoll-Paque (GE Healthcare Life Sciences, Pittsburgh, PA), resuspended in 90% fetal bovine serum (Thermo Fisher Scientific, Waltham, MA) and 10% dimethyl sulfoxide (Sigma Aldrich, St. Louis, MO) and stored at −140°C until use. Mononuclear cell viability, determined by Trypan Blue exclusion, exceeded 98%.

Autoptic tissue samples were placed in formalin immediately after collection; after 24 hours, samples were processed and paraffin embedded. Formalin fixed paraffin embedded (FFPE) tissue samples were kept at 4°C until RNA was extracted.

RNA extraction and NanoString transcriptomic profiling

Total RNA was obtained from PBMC and FFPE samples using the RNeasy Mini kit (Qiagen, Germantown, MD) and the AllPrep DNA/RNA FFPE kit according to the manufacturer's instructions. RNA quantification was carried out using Nanodrop whereas RNA integrity was verified using Agilent Bioanalyzer. Samples with DN200 higher than 70% were used for subsequent steps. NanoString profiling was performed using the nCounter Human CAR-T characterization panel. 100 ng of total RNA was used as input into hybridization reactions containing reporter and capture probes, according to the manufacturer's instructions. RNA samples were hybridized at 65°C for 24 hours and subsequently processed and each analyzed in a single nCounter cartridge lane. Post hybridization processing was carried out in an nCounter MAX System. RCC files were compiled and analyzed using nSolver analysis software (version 4.0), as per instructions of the manufacturer. The internal reference genes included in the probe set were used for normalization. All PBMC and FFPE samples subjected to NanoString analysis were run in triplicate and experiments repeated independently three times.

qPCR

Expression of human *CD39* mRNA and *CD39-AS* RNA was determined by qRT-PCR. Total RNA was obtained from PBMC and FFPE samples, as indicated above. mRNA was reverse transcribed using iScript cDNA synthesis kit (Bio-Rad Laboratories, Hercules, CA) according to the manufacturer's instructions. *ENTPD1/CD39* and antisense primer sequences are as follows:

CD39/ENTPD1

Forward 5′ AGGTGCCTATGGCTGGATTAC 3′

Reverse 5′ CCAAAGCTCCAAAGGTTTCCT 3′

CD39-AS

Forward 5′ AATACTGTGACACTGACCACCAGG 3′

Reverse 5′ TGAATCCACTCTGTCTCCTGCA 3′

Samples were run in triplicate on a QuantStudio 3 (Applied Biosystems, Foster City, CA). Experiments were repeated independently three times. Results were analyzed by matched software and expressed as relative quantification. Relative gene expression was determined after normalization to human β-actin.

Immunohistochemistry

Paraffin embedded lung, heart, liver, kidney, and spleen tissue sections were subjected to antigen retrieval (Liberal et al., 2016). Sections were subsequently incubated overnight at 4°C with rabbit polyclonal anti-human CD39 (cat. # HPA014067, Sigma Aldrich) at 1/100 (Vuerich et al., 2021). Following endogenous peroxidase blocking with 3% H_2O_2, sections were incubated with 1/1,000 goat anti-rabbit secondary antibody (Vector Laboratories, Burlingame, CA) for one hour at room temperature. After treatment with Vectastain Elite ABC kit (Vector Laboratories), ImmPACT DAB (Vector Laboratories) was applied and sections examined by light microscopy.

Flow cytometry

PBMCs were stained with PerCP-Cyanine 5.5 anti-human CD4 (clone # OKT4, Biolegend, San Diego, CA), PE anti-human CD8 (clone # SK1, Biolegend), FITC anti-human TCR V alpha 2 (clone # F1, Invitrogen, Waltham, MA) and FITC anti-human TCR V beta 3.1 (clone # 8F10, Invitrogen). Cells were acquired on a CytoFLEX LX flow cytometer (Beckman Coulter, Pasadena, CA) and analyzed using FlowJo 2 software (version 10, TreeStar, Ashland, OR). Fluorescence compensation was adjusted based on fluorescence-minus-one method.

QUANTIFICATION AND STATISTICAL ANALYSIS

R software (version 4.0.2) was used for further data analysis of normalized data, differentially expressed gene (DEG) results and gene set scores obtained from nSolver Advanced Analysis software. Heatmaps of DEGs were obtained using pheatmap package. DEGs where defined based on P value $\leq 10^{-4}$ when analyzing samples from organs; and P value $\leq 10^{-3}$ when analyzing PBMC samples. Two different threshold for P values were adopted because the changes in gene expression were more substantial in the organs than PBMC samples. False-discovery-rate (FDR) was controlled by the Benjamini-Yekutieli method. All DEGs had FDR consistently lower than 0.05.

When subdividing the genes of the nCounter CAR-T Characterization Panel based on high and low *ENTPD1* expression levels (high and low *ENTPD1* expression was based on the median expression levels in severe and convalescent COVID-19 patients), limma package was used (Ritchie et al., 2015). For this set of analysis, genes with a P value < 0.05 and a |Log fold change| > 0.585 were defined as DEGs.

To identify enriched pathways, GSEA was carried out on the pathway annotations included in the nCounter CAR-T Characterization Panel and visualized using clusterProfiler package (Yu et al., 2012). Gene sets with nominal P value < 0.05 and FDR q value < 0.05 were considered significant. Pathway enrichment results were also visualized using enrichplot package (Yu et al., 2012).

Protein-protein interaction (PPI) network was retrieved from the STRING database using a threshold value of median confidence of 0.4. Results were inputted and analyzed using Cytoscape software (version 3.8.2) (Shannon et al., 2003). Cytohubba plugin in Cytoscape was used to visualize the relationships within the PPI network, based on the degree ranking in Cytoscape.

qPCR and flow cytometry data are presented as Mean $\pm$ SEM. Normality of variable distribution was assessed by Kolmogorov-Smirnov goodness-of-fit test. Comparisons were performed using unpaired Student's *t* test. One-way ANOVA test, followed by Tukey's multiple comparison test, were used when comparing more than two sets of data. Correlation analysis was performed using Pearson's correlation coefficient. P $\leq$ 0.05 was considered significant. Statistical analysis was performed using GraphPad Prism, version 7.0a (GraphPad Software, San Diego, CA).